Ceramics International 46 (2020) 23813–23819

Contents lists available at ScienceDirect

Ceramics International

journal homepage: www.elsevier.com/locate/ceramint

Enhanced tribological properties of Y/MoS_2 composite coatings prepared by chemical vapor deposition

J. Yi[a,1], M.L. Li[b,1], H.X. Zhou[b,***], Andreas Rosenkranz[c,**], B. Wang[a,*], H. Song[a], N. Jiang[a]

[a] Key Laboratory of Marine Materials and Related Technologies, Zhejiang Key Laboratory of Marine Materials and Protective Technologies, Ningbo Institute of Materials Technology and Engineering, Chinese Academy of Sciences, Ningbo, 315201, China

[b] School of Energy and Power Engineering, Dalian University of Technology, Dalian, 116024, China

[c] Department of Chemical Engineering, Biotechnology and Materials, Faculty of Physical and Mathematical Sciences, University of Chile, Beauchef 851, Santiago, Chile

ARTICLE INFO

Keywords:
CVD
MoS_2
Composite coatings
Solid lubrication

ABSTRACT

Chemical vapor deposition (CVD) is an efficient approach to prepare coatings on complex cutting tools. However, MoS_2 with self-lubrication ability and excellent tribological properties fabricated by CVD have been rarely reported in literature. The aim of this study was to deposit pure MoS_2 coatings and yttrium (Y) doped MoS_2 (Y/MoS_2) composite coatings on cemented carbide blades coated with titanium nitride by CVD. The structural and mechanical properties of the coatings were examined by scanning electron microscopy (SEM) and nanoindentation, respectively. The results demonstrated that the microstructure of Y/MoS_2 composite coatings was denser than that of the pure MoS_2 coating. The hardness and the adhesional properties were significantly enhanced for the Y/MoS_2 composite coatings. The tribological performance of the as-deposited coatings were investigated under atmospheric environment. Y/MoS_2 compostite coatings demonstrated an enhanced tribological performance with a stable and low coefficient of friction (COF) over the entire sliding time. In contrast, the COF of pure MoS_2 coating dramatically increased to value above 0.3 after a sliding time of only 30 min. Additionally, the Y/MoS_2 composite coatings showed a decreased wear rate ($8.36 \pm 0.29 \times 10^{-7}$ mm^3/Nm) compared to the pure MoS_2 coatings ($3.41 \pm 0.48 \times 10^{-5}$ mm^3/Nm) thus reflecting an improvement by two order of magnitude.

1. Introduction

Cemented carbide blades coated with titanium nitride (TiN) are widely used in metal processing [1–3]. Since the service life of TiN coatings drastically decreases under severe conditions, such as dry machining and elevated loads [2–6], it is imperative to develop efficient strategies to enhance the wear resistance and the tribological properties. Thus, soft MoS_2 coatings with self-lubrication ability are deposited on “harder” TiN coatings to reduce friction and to decrease the resulting cutting forces as well as cutting temperatures during machining. Using this approach, the service life of TiN coatings can be greatly improved [1,7–11].

MoS_2 coatings are typically deposited using magnetron sputtering [1,7–10], atomic layer deposition (ALD) [11], laser cladding [12], among others. However, techniques based upon CVD may have certain advantages compared to PVD-based approaches such as low cost and the ability to coat complex tools [13–18]. However, only a limited number of studies have reported on the successful deposition of MoS_2 coatings by CVD [19–21]. Although the fabrication of mono-layer MoS_2 films by CVD has recently become hotspot due to their outstanding electrical properties [22–27], experimental studies addressing the friction and wear performance of CVD-deposited MoS_2 coatings have not been reported yet.

Therefore, the aim of this study was to deposit pure MoS_2 coatings and Y/MoS_2 composite coatings on cemented carbide blades by CVD with the ultimate goal to enhance the tribological properties. In this context, the microstructure and surface chemistry of the as-deposited coatings were studied in detail. Subsequently, the tribological performance of the fabricated coatings was investigated using a ball-on-disk tribometer under atmospheric conditions.

[*] Corresponding author.
[**] Corresponding author.
[***] Corresponding author.
E-mail addresses: hxzhou@dlut.edu.cn (H.X. Zhou), arosenkranz@ing.uchile.cl (A. Rosenkranz), wangb@nimte.ac.cn (B. Wang).
[1] These authors contributed equally to this work.

https://doi.org/10.1016/j.ceramint.2020.06.157
Received 31 May 2020; Received in revised form 12 June 2020; Accepted 15 June 2020
Available online 18 June 2020
0272-8842/

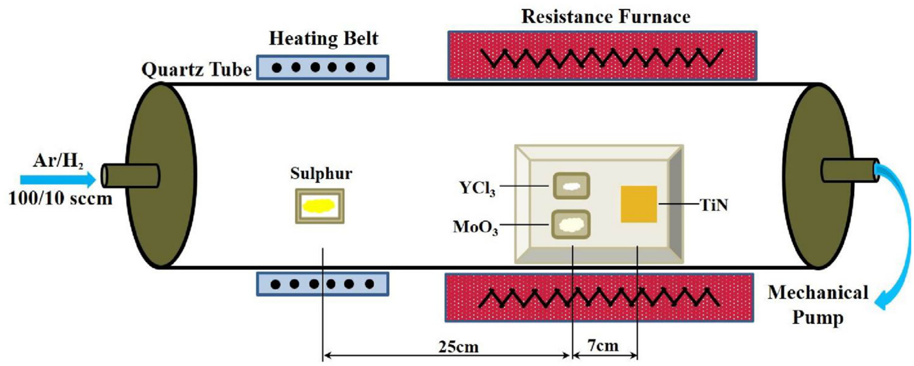

Fig. 1. Schematic diagram of the experimental set-up to prepate the respective coatings.

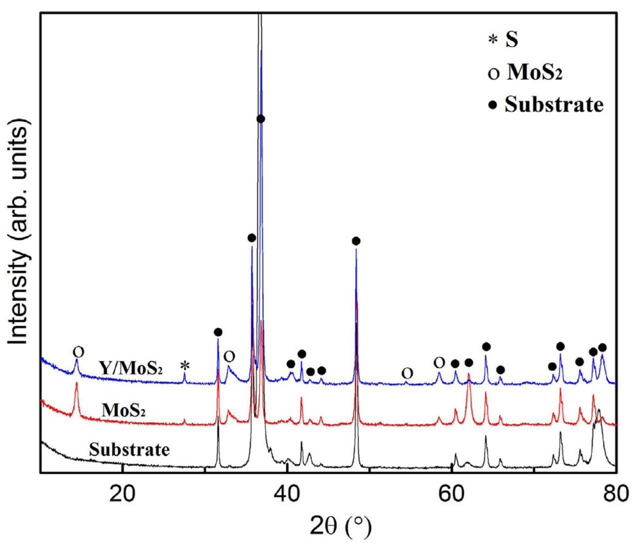

Fig. 2. XRD patterns of the substrate, the pure MoS_2 and the Y/MoS_2 coating.

2. Experimental details

Commercially available cemented carbide blades coated with TiN (Zhuzhou, China) have been used as substrate materials. Commercial sulphur (S), yttrium trichloride hexahydrate ($YCl_3{\cdot}6H_2O$) and molybdenum trioxide (MoO_3) powder were obtained from Aladdin. The trichloride hexahydrate powder was dried to generate YCl_3 powder prior to the experiments. As shown in Fig. 1, S, YCl_3 and MoO_3 were used as precursors. After pumping the tube furnace to 1.6 Pa, the tube was heated using a heating rate of 20 °C/min under a mixed argon/hydrogen atmosphere (100:10, sccm). After temperature reaching 700 °C, the heating rate was reduced to 5 °C/min until reaching the final temperature of 820 °C. In the meantime, S powder was heated to 130 °C by a heating belt. Afterwards, Y/MoS_2 composite coatings were deposited at 820 °C for 2 h under a furnace pressure of 2 kPa. In order to deposit pure MoS_2 coatings, the experimental conditions were kept constant, but only S and MoO_3 were used as precursors. The thickness of the two kind of as-deposited coatings were similar and about 1.4 μm.

The microstructure of the as-deposited coatings surface was examined by scanning electron microscopy (SEM, Hitachi S-4800), energy dispersive spectroscopy (EDS, Oxford Inca Energy 250) and high-resolution transmission electron microscopy (HRTEM, FEI Tecnai F20). TEM samples were prepared using focused ion beam microscopy (FIB, Auriga, Germany). The phase analysis of the as-deposited coatings were studied by X-ray diffraction (XRD, Bruker AXS D8) using CuKα radiation. The surface chemistry of the as-deposited coatings was analyzed by X-ray photoelectron spectroscopy (XPS, Axis ultraDLD) and Raman spectroscopy (Renishaw) with 532 nm laser. The hardness and adhesional properties of the as-deposited coatings were characterized using nanoindentation (MTS NanoIndenter G200) and scratch testing (Revetest), respectively.

The tribological properties of the as-deposited coatings were studied using a ball-on-disk tribometer (Rtec MFT-5000) under atmospheric conditions with a relative humidity (RH) of about 75–80%. The counter-body was a GCr15 steel ball (HRC 60) with a diameter of 6 mm. All tribological tests were carried out using a sliding speed of 20 mm/s and a normal load of 5 N. The stroke length was set to 5 mm with a frequency of 2 Hz under linear reciprocating motion. The total sliding time was set to 3 h (10,800 s). The tribological tests were stopped once the coefficient of friction (COF) exceeded a value of 0.3. After the tribological tests, the morphology of the worn surfaces was characterized using confocal laser scanning microscopy (CLSM). The wear rates (k) of the as-deposited coatings were calculated based upon the measured wear volumes using CLSM.

3. Results and discussion

3.1. Microstructural analysis of the coatings

The resulting crystallinity and phases of the as-deposited coatings were analyzed by XRD (Fig. 2). The diffraction peaks located at 13, 33 and 59°can be related to the (002), (100) and (110) crystal planes of MoS_2, thus proving the successful deposition of MoS_2 coatings. In addition, a diffraction associated to S can be observed in the XRD patterns of the as-deposited coatings, which can be explained by an excess of S during deposition. However, no individual diffraction peak of Y can be seen in the XRD pattern of the doped composite coating, which is probably due to the limited amount of Y in the composite coating.

Fig. 3 depicts the microstructure of the as-deposited coatings. The pure MoS_2 coating reveals a rather loose microstructure composed of parallel MoS_2 flakes and S particles, which can be well recognized in the given EDS analysis shown in insets of A and B (Fig. 3(a)). In contrast, the Y/MoS_2 composite coating depicts a denser microstructure composed of disordered MoS_2 flakes and S particles wrapped in little MoS_2 flakes, which can be seen in EDS analysis shown in the insets of C and D (Fig. 3(b)). Consequently, the addition of the rare earth element Y changed the growth mechanism of MoS_2 coatings and helped to optimize their microstructure.

Fig. 4 reveals the HR-TEM images of the as-deposited coatings. Fig. 4(a) reveals a parallel oriented, layered structure with a layer spacing of 6.16 Å, which is related to MoS_2. The inset in Fig. 4(a) is the corresponding selected area electron diffraction (SAED) pattern, which shows a typical polycrystalline pattern. As depicted in the SAED pattern, these diffraction cycles can be assigned to {002}, {001} and {110} planes of MoS_2, which are consistent with the HRTEM results. For the Y/MoS_2 composite coating, a similar layered structure with the same spacing of 6.16 Å can be seen in Fig. 4(b). The SAED (the inset in

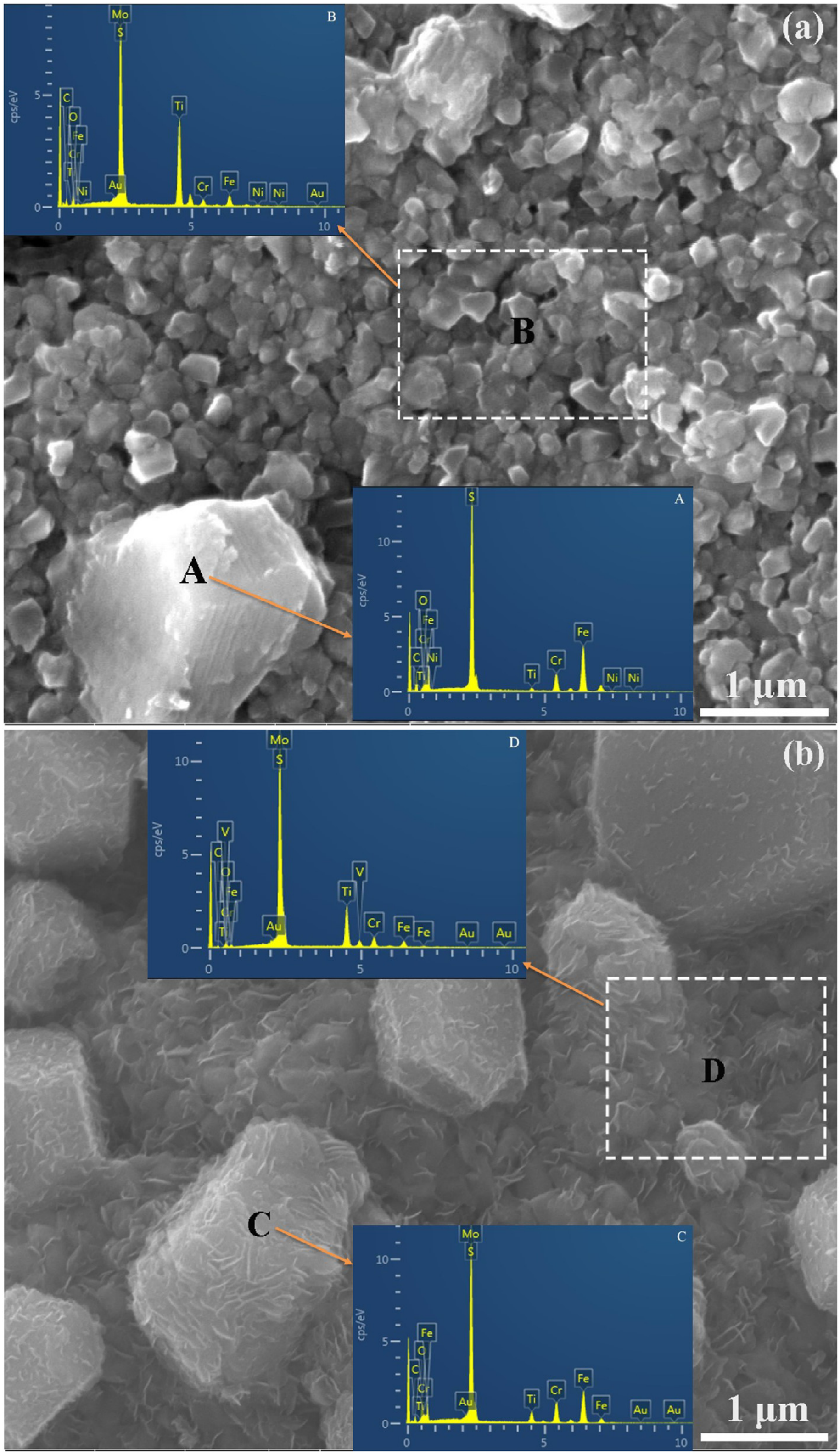

Fig. 3. SEM micrographs of (a) the pure MoS_2 coating and (b) the Y/MoS_2 coating, while the insets show the respective EDS analysis for both coatings.

Fig. 4(b)) also verifies the polycrystalline nature of Y/MoS_2 composite coating.

3.2. Chemical characterization of the coatings

Fig. 5 shows the measured Raman spectra for the as-deposited coatings. The strong peaks located at around 380 and 410 cm^{-1} can be related to the E^1_{2g} and A_{1g} peaks of MoS_2, respectively. Weaker peaks of MoO_2 and MoO_3 can be also observed in Raman spectra, which indicates that small quantities of MoO_2 and MoO_3 are present in the as-deposited coatings.

Fig. 6 shows the measured data of the S_{2p}, Mo_{3d} and Y_{3d}

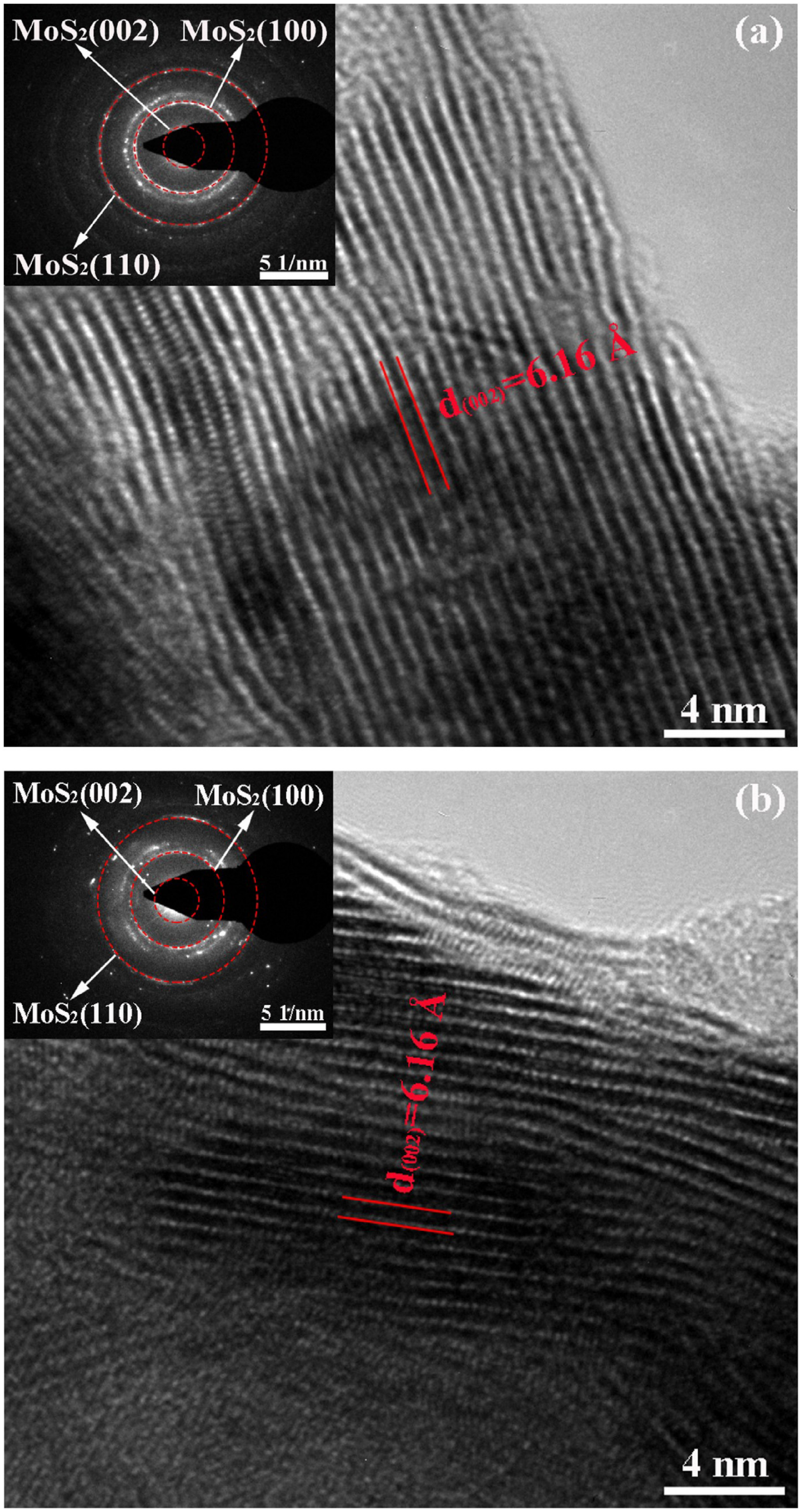

Fig. 4. HR-TEM images: (a) pure MoS_2 coating, (b) Y/MoS_2 coating.

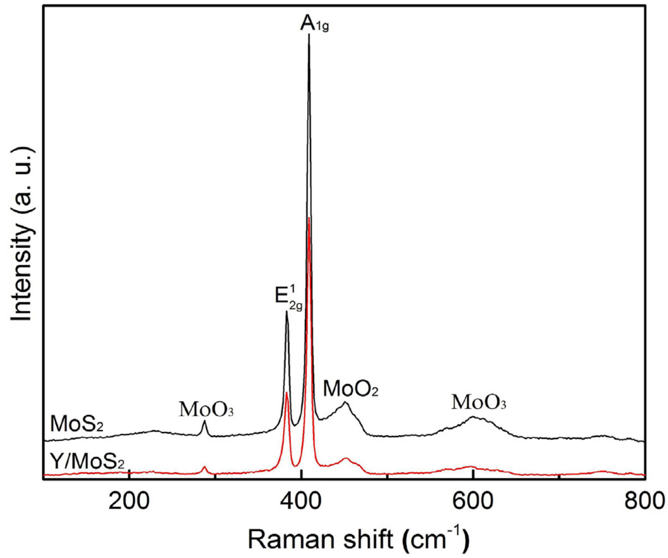

Fig. 5. Obtained Raman spectra of the MoS_2 and Y/MoS_2 coatings.

photoelectron peaks. The contributions of the S_{2p} peak located at 162.1 and 163.3 eV (Fig. 6(a)) as well as the contributions of the Mo_{3d} peak centered at 229.3 and 232.4 eV (Fig. 6(b)) can be attributed to MoS_2 [10]. When comparing both coatings, it can be observed that the peaks of the S_{2p} and Mo_{3d} peaks are narrower for the Y/MoS_2 composite coating. This implies that S and Mo in Y/MoS_2 composite coatings have less chemical bonds than in the pure MoS_2 coating. Based upon that, it can be assumed that the MoS_2 in the Y/MoS_2 composite coating is purer compared to that in MoS_2 coating. The contributions of the Y_{3d} peak located at 157.2 and 159.8 eV are rather broad with low intensities, which goes hand in hand with the low amount of Y in the Y/MoS_2 composite coatings thus confirming the XRD results (Fig. 2).

3.3. Mechanical properties of the coatings

The hardness and adhesional strength of the as-deposited coatings have been investigated. As summarized in Table 1, the hardness of the pure MoS_2 coating is about 3.3 ± 0.1 GPa, while the hardness of the Y/MoS_2 composite coating is approximiately 7.5 ± 0.4 GPa, which implies an increase in hardness of almost a factor of 2.5. The coating-substrate adhesion of pure MoS_2 is only 3 ± 0.3 N, while the respective values for the Y/MoS_2 composite coating reaches 50 ± 0.9 N, which reflects a 16-fold improvement. This can be traced back to the denser microstructure of the Y/MoS_2 composite coating, which agrees well with the SEM results (Fig. 3). Overall, these results demonstrate that the addition of the rare earth element Y greatly improved the hardness and coating-substrate adhesion of the Y/MoS_2 coating.

3.4. Tribological properties of the coatings

Fig. 7 shows the temporal evolution of the COF for both coatings. As can be seen in Fig. 7, the COF of the substrate is rather high and exceeds values of 0.5 after a sliding time of 100 s. The COF of the pure MoS_2 coating started to increase suddenly after 30 min thus exceeding COF values of 0.3. This experimental trend reflects well the poor anti-wear resistance of these coatings and agrees well with published studies in the literature [19–21]. The initial COF of the Y/MoS_2 composite coating is about 0.07. After a slight increase, the COF stays fairly constant for the entire measuring time thus reaching a COF of 0.128 after 3 h. This performance is comparable and competitive to the performance of doped MoS_2 coatings prepared by PVD [7–10].

The worn surfaces after the tribological experiments were characterized by CLSM using 3D profile plots. As can be observed in

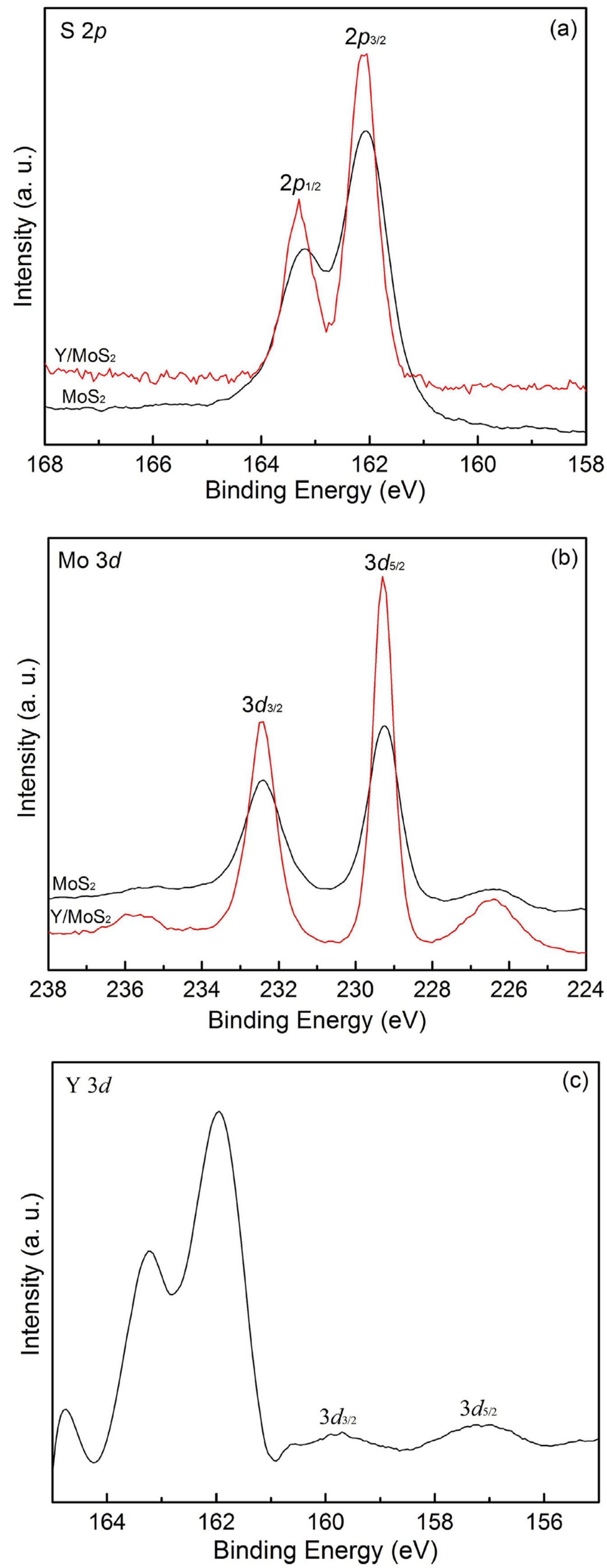

Fig. 6. XPS analysis of the (a) S_{2p}, (b) Mo_{3d} and (c) Y_{3d} peaks for both coatings. Please note that in case of the Y_{3d} peak, only the doped coating is shown.

Table 1
Summary of the obtained hardness and adhesion strength for the as-deposited coatings.

Mechanical Property	MoS_2	Y/MoS_2
Hardness/GPa	3.3 ± 0.1	7.5 ± 0.4
Critical load/N	3 ± 0.3	50 ± 0.9

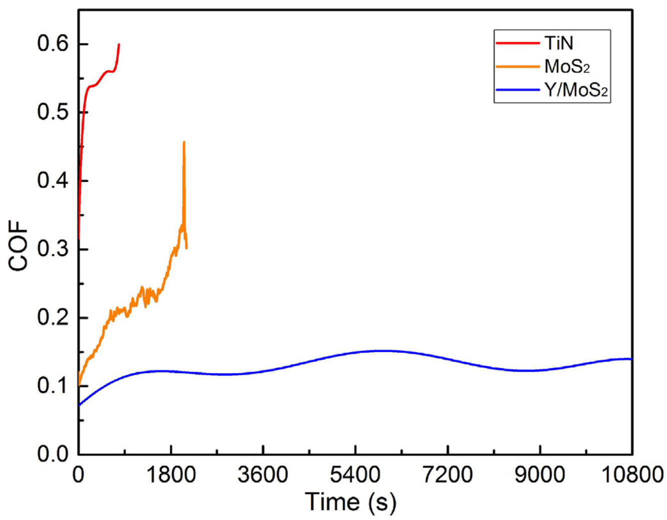

Fig. 7. Temporal evolution of the COF for the substrate and both fabricated coatings.

Fig. 8(a), the wear track of pure MoS_2 coating is considerably deep and wide, thus demonstrating pronounced ploughing grooves at the right edge of the wear track. The wear track of the Y/MoS_2 composite coating is notably shallower and narrower with only limited ploughing marks caused by abrasive wear. Moreover, the wear rates of the as-deposited coatings were calculated after the tribological tests. The wear rates of the pure MoS_2 coating and the Y/MoS_2 composite coating can be given as $3.41 \pm 0.48 \times 10^{-5}$ and $8.36 \pm 0.29 \times 10^{-7}$ mm^3/Nm, respectively. These results indicate an improvement in the wear rate by almost two order of magnitude induced by the addition of Y. Together with the stable evolution of the COF, this underlines the excellent friction and anti-wear performance of the Y/MoS_2 composite coatings. The results of CLSM are consistent with results of the microstructural and mechanical characterization of the as-deposited coatings thus verifying that the addition of rare earth element Y greatly improves their mechanical and tribological properties.

4. Conclusion

Pure MoS_2 coatings and Y/MoS_2 composite coatings have been successfully deposited by CVD on commercial cemented carbide blades coated with titanium nitride. The addition of the rare earth element Y induced a denser microstructure of MoS_2 coating. Moreover, the addition of rare earth element Y greatly improved the mechanical properties thus leading to an increased hardness and enhanced coating-substrate adhesion. As a consequence, the tribological properties of the Y/MoS_2 composite coatings are greatly enhanced, thus demonstrating a low and stable COF and an improved wear resistance. The COF of the Y/MoS_2 composite coating is still as low as 0.128 after a sliding time of 3 h. The wear rate showed an improvement of about two order of magnitude compared to the pure MoS_2 coatings. These results can compete with the existing state-of-the-art doped MoS_2 coatings fabricated by PVD.

Declaration of competing interest

The authors declare that they have no known competing financial interests or personal relationships that could have appeared to

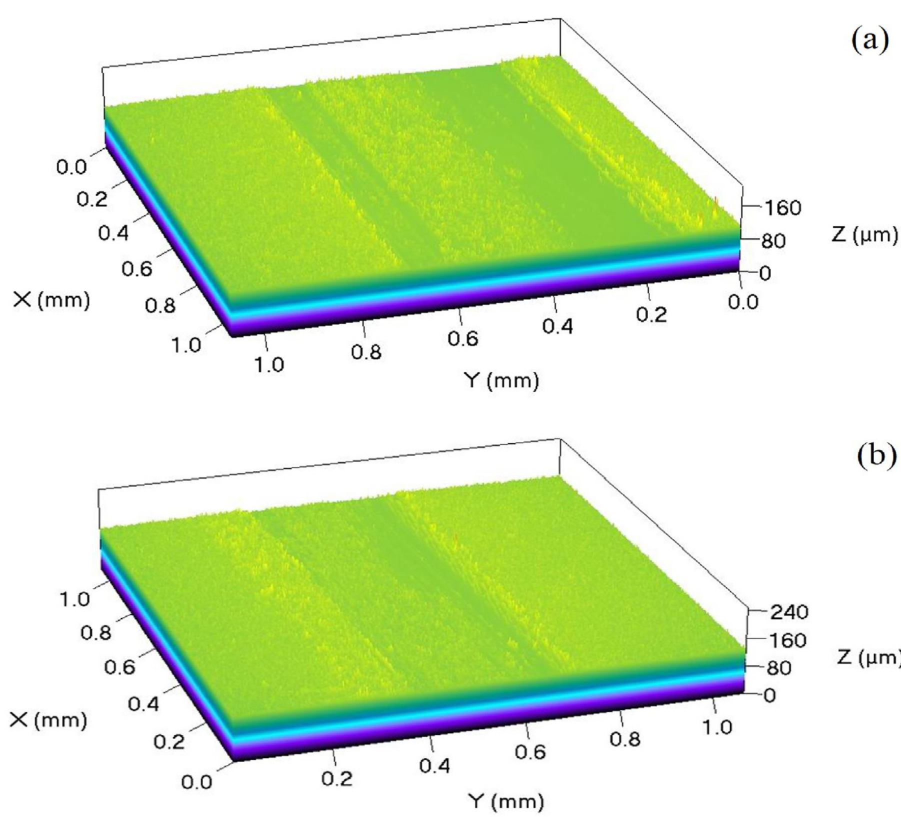

Fig. 8. Characterization of the worn surfaces using CLSM: (a) MoS_2 coating, (b) Y/MoS_2 coating.

influence the work reported in this paper.

Acknowledgements

This work was supported by the National Key Research and Development Project (No. 2017YFE0128600), National Natural Science Foundation of China (Grant No. 51705482), Ningbo 3315 Innovation Team (Y90331DL02), Science and Technology Innovation 2025 Major Project of Ningbo (No. 2018B10046), National Defense Key Laboratory Fund (Nos. 6142807180511 and 6142905192806), Innovation Funding of State Oceanic Administration (No. NBHY-2017-Z3), Ningbo Industrial Technology Innovation Project (No. 2016B10038), Foundation of State Key Laboratory of Solid lubrication (LSL-1912), and 'Key Talents' Senior Engineer Project of Ningbo Institute of Materials Technology and Engineering. B. Wang, N. Jiang and Andreas Rosenkranz gratefully acknowledge the financial support of Chinese Academy of Sciences President's International Fellowship Initiative (2020VEC0006). A. Rosenkranz gratefully acknowledges ANID-CHILE for the financial support given in the project Fondecyt 11180121 and the VID of the University of Chile in the framework of "U-Inicia UI013/2018".

References

[1] M.S. Libório, G.B. Praxedes, L.L.F. Lima, I.G. Nascimento, R.R.M. Sousa, M. Naeem, et al., Surface modification of M2 steel by combination of cathodic cage plasma deposition and magnetron sputtered MoS_2-TiN multilayer coatings, Surf. Coating. Technol. 384 (2020) 125327.

[2] M. Meindlhumer, N. Jäger, S. Spor, M. Rosenthal, J.F. Keckes, H. Hruby, et al., Nanoscale residual stress and microstructure gradients across the cutting edge area of a TiN coating on WC-Co, Scripta Mater. 182 (2020) 11–15.

[3] S.S. Malvajerdi, A.S. Malvajerdi, M. Ghanaatshoar, Protection of CK45 carbon steel tillage tools using TiN coating deposited by an arc-PVD method, Ceram. Int. 45 (2019) 3816–3822.

[4] A. Vereschaka, V. Tabakov, S. Grigoriev, N. Sitnikov, F. Milovich, Investigation of the influence of the thickness of nanolayers in wear-resistant layers of Ti-TiN-(Ti,Cr,Al)N coating on destruction in the cutting and wear of carbide cutting tools, Surf. Coating. Technol. 385 (2020) 125402.

[5] R.F. Avila, R.D. Mancosu, A.R. Machado, S.D. Vecchio, R.B. daSilva, J.M. Vieira, Comparative analysis of wear on PVD TiN and $(Ti_{1-x}Al_x)N$ coatings in machining process, Wear 302 (2013) 1192–1200.

[6] S. Kumar, S.R. Maity, L. Patnaik, Effect of heat treatment and TiN coating on AISI O1 cold work tool steel. Mater. Today: Proceedings (In press).

[7] R. Zhang, X. Yang, J. Pu, Z. He, L. Xiong, Extraordinary macroscale lubricity of sonication-assisted fabrication of MoS_2 nano-ball and investigation of in situ formation mechanism of graphene induced by tribochemical reactions, Appl. Surf. Sci. 510 (2020) 145456.

[8] X. Zhao, Z. Lu, G. Zhang, L. Wang, Q. Xue, Self-adaptive MoS_2-Pb-Ti film for vacuum and humid air, Surf. Coating. Technol. 345 (2018) 152–166.

[9] Y. Bai, J. Pu, H. Wang, L. Wang, Q. Xue, S. Liu, High humidity and high vacuum environment performance of MoS_2/Sn composite film, J. Alloys Compd. 800 (2019) 107–115.

[10] K. Shang, S. Zheng, S. Ren, J. Pu, D. He, S. Liu, Improving the tribological and corrosive properties of MoS_2-based coatings by dual-doping and multilayer construction, Appl. Surf. Sci. 437 (2018) 233–244.

[11] Y. Xing, Z. Wua, J. Yang, X. Wang, L. Liu, LIPSS combined with ALD MoS_2 nano-coatings for enhancing surface friction and hydrophobic performances, Surf. Coating. Technol. 385 (2020) 125396.

[12] C.C. Qu, J. Li, Y.F. Juan, J.Z. Shao, R. Song, et al., Effects of the content of MoS_2 on microstructural evolution and wear behaviors of the laser-clad coatings, Surf. Coating. Technol. 357 (2019) 811–821.

[13] S. Dasa, S. Guhab, P.P. Dasa, R.K. Ghadai, Analysis of morphological, micro-structural, electrochemical and nano mechanical characteristics of TiCN coatings prepared under N_2 gas flow rate by chemical vapour deposition (CVD) process at higher temperature, Ceram. Int. 46 (2020) 10292–10298.

[14] Q. He, J.M. Paiv, J. Kohlscheen, B.D. Beake, S.C. Veldhuis, An integrative approach to coating/carbide substrate design of CVD and PVD coated cutting tools during the machining of austenitic stainless steel, Ceram. Int. 46 (2020) 5149–5158.

[15] C. Kainz, N. Schalk, M. Tkadletz, C. Mitterer, C. Czettl, Microstructure and mechanical properties of CVD TiN/TiBN multilayer coatings, Surf. Coating. Technol. 370 (2019) 311–319.

[16] D. Ma, T.J. Harvey, Y.N. Zhuk, R.G. Wellman, R.J.K. Wood, Cavitation erosion performance of CVD W/WC coatings, Wear 452–453 (2020) 203276.

[17] S. Saketi, M. Olsson, Influence of CVD and PVD coating micro topography on the initial material transfer of 316L stainless steel in sliding contacts-A laboratory study, Wear 388–389 (2017) 29–38.

[18] T. Shen, L. Zhu, Z. Liu, Effect of micro-blasting on the tribological properties of TiN/MT-TiCN/Al_2O_3/TiCNO coatings deposited by CVD, Int. J. Refract. Met. H. 88 (2020) 105205.

[19] Y.W. Bae, W.Y. Lee, C.S. Yust, J. Blau, T.M. Bes, Synthesis and friction behavior of chemically vapor deposited composite coatings containing discrete TiN and MoS_2 phases, J. Am. Ceram. Soc. 79 (1996) 819–824.

[20] Y.W. Bae, W.Y. Lee, T.M. Besmann, C.S. Yust, P.J. Blau, Preparation and friction characteristics of self-lubricating TiN-MoS_2 composite coatings, Mater. Sci. Eng., A 209 (1996) 372–376.

[21] I. Endler, A. Leonhardt, U. Konig, H. Berg, W. Pitschke, V. Sottke, Chemical vapour deposition of MoS_2 coatings using the precursors $MoCl_5$ and H_2S, Surf. Coating. Technol. 120–121 (1999) 482–488.

[22] R. Shidpour, S.M.S. Movahed, Identification of defective two dimensional semi-conductors by multifractal analysis: the single-layer MoS_2 case study, Phys. A 508 (2018) 757–770.

[23] J. Guo, R. Wen, J. Zhai, Z.L. Wang, Enhanced NO_2 gas sensing of a single-layer MoS_2 by photogating and piezo-phototronic effects, Sci. Bull. 64 (2019) 128–135.

[24] V.K. Sangwan, H.S. Lee, H. Bergeron, I. Balla, M.E. Beck, et al., Multi-terminal memtransistors from polycrystalline monolayer molybdenum disulfide, Nature 554 (2018) 500–504.

[25] X. Chen, Y.J. Park, M. Kang, S.K. Kang, J. Koo, CVD-grown monolayer MoS_2 in bioabsorbable electronics and biosensors, Nat. Commun. 9 (2018) 1690.

[26] R. Luo, W.W. Xu, Y. Zhang, Z. Wang, X. Wang, Van der Waals interfacial reconstruction in monolayer transition-metal dichalcogenides and gold heterojunctions, Nat. Commun. 11 (2020) 1011.

[27] O. Zheliuk, J.M. Lu, Q.H. Chen, A.A.E. Yumin, S. Golightly, J.T. Ye, Josephson coupled Ising pairing induced in suspended MoS_2 bilayers by double-side ionic gating, Nat. Nanotechnol. 14 (2019) 1123–1128.